INTEGRATED VEHICLE AND TRAJECTORY DESIGN OF SMALL SPACECRAFT WITH ELECTRIC PROPULSION FOR EARTH AND INTERPLANETARY MISSIONS

Sara Spangelo
Jet Propulsion Laboratory, California Institute of Technology
4800 Oak Grove Drive, Pasadena, CA 91109; 1-818-354-0699
Sara.Spangelo@jpl.nasa.gov

Derek Dalle
Ames Research Center
Mail Stop 258-2, Moffett Field, CA;
derek.j.dalle@nasa.gov

Benjamin Longmier
Department of Aerospace Engineering, University of Michigan
3017 FXB Building, 1320 Beal Ave, Ann Arbor, MI 48109;
longmier@umich.edu

ABSTRACT

This paper investigates the feasibility of Earth-transfer and interplanetary mission architectures for miniaturized spacecraft using emerging small solar electric propulsion technologies. Emerging small SEP thrusters offer significant advantages relative to existing technologies and will enable U-class systems to perform trajectory maneuvers with significant ΔV requirements. The approach in this paper is unique because it integrates trajectory design with vehicle sizing and accounts for the system and operational constraints of small U-class missions. The modeling framework includes integrated propulsion, orbit, energy, and external environment dynamics and systems-level power, energy, mass, and volume constraints. The trajectory simulation environment models orbit boosts in Earth orbit and flyby and capture trajectories to interplanetary destinations. A family of small spacecraft mission architectures are studied, including altitude and inclination transfers in Earth orbit and trajectories that escape Earth orbit and travel to interplanetary destinations such as Mercury, Venus, and Mars. Results are presented visually to show the trade-offs between competing performance objectives such as maximizing available mass and volume for payloads and minimizing transfer time. The results demonstrate the feasibility of using small spacecraft to perform significant Earth and interplanetary orbit transfers in less than one year with reasonable U-class mass, power, volume, and mission durations.

INTRODUCTION

Motivation

Small electric propulsion (SEP) technologies are game-changing because they will enable small spacecraft to perform large orbital transfers in Earth orbit, form and maintain large apertures or constellations, drag make-up, proximity operations, hovering (over comets, asteroids, moons), and achieving precision pointing in both Earth orbit and interplanetary destinations*. For the first time, small spacecraft will no longer be passive drifters and instead be able to accomplish SMEX to Discovery-class science, and travel to dangerous and unexplored regions of the solar system like Earth-Sun L4/L5, comets, or moons like Europa as precursor missions for a fraction of the cost of conventional mission architectures [1, 2]. Furthermore, an increasing number of CubeSats are being proposed for constellations [3, 4], where propulsion capabilities are required or highly desired. SEP is attractive for many missions because most thrusters can operate over a range of power values, which can enable a mission to adopt to available energy either due to operational demands or distance from the Sun for interplanetary transfers, however the efficiency often decreases at lower power values. SEP thrusters can also be turned on and off to perform multiple maneuvers throughout the mission, however for many technologies minimizing the number of times the thruster is turned on is important to extend lifetime. Large orbit transfers are particularly challenging for

*www.lpi.usra.edu/meetings/marsconcepts2012/pdf/4277.pdf+&cd=8&hl=en&ct=clnk&gl=us

small spacecraft low-thrust propulsion systems because typical high-thrust maneuvers can not be utilized and small spacecraft are extremely mass, volume, and power constrained [5]. Furthermore, CubeSats do not typically operate at the high power or high voltage levels required to support propulsion systems, nor do small spacecraft have solutions for managing the high thermal loads (CubeSats typically use passive thermal control techniques). Therefore, it is particularly critical to consider a systems-level approach in the design optimization of small spacecraft vehicles and their trajectory maneuvers, which is the focus of this paper.

Most existing electric propulsion systems exceed the mass and/or volume envelopes for U-class spacecraft, have low efficiency or low thrust, or are designed for precise pointing maneuvers. However, recent technology advancements in miniaturized propulsion systems, such as the University of Michigan/Aether's CubeSat Ambipolar Thruster (CAT) [6], UCLA/JPL's Miniature Xenon Ion (MiXI) [7], and the three Micro Electrospray Propulsion (MEP) technologies being funded by STMD[†]: JPL's MEP thruster, MIT's scalable Ion Electrospray Propulsion System (S-iEPS), and Busek's MEP thruster [5], are being developed to produce large amounts of thrust and ΔV, while satisfying the size, mass, power, thermal, and launch constraints of small spacecraft. Key performance parameters for these emerging technologies will be presented in this paper, however the examples focus on the CAT thruster due to its high performance and availability of technical parameters. The general approach presented in this paper is applicable to all other technologies.

SEP technologies are enabled by the considerable CubeSat flight heritage in Low Earth Orbit (LEO) as well as the upcoming launch and mission opportunities for CubeSats to operate and perform ambitious science and technology goals beyond Earth orbit, including for planetary [8], astrophysics, and heliophysics [‡] science applications. Flying small SEP thrusters is also enabled by considerable advances in telecommunication and navigation technologies, high accuracy attitude determination and control systems, high-efficiency body-fixed and deployable solar arrays, and the emergence of integrated bus architectures and radiation-tolerant U-class components [9]. Many of these components are Commercial Off-The-Shelf (COTS) and can be purchased for low-cost and integrated relatively easily into U-class spacecraft architectures.

[†] https://gcd.larc.nasa.gov/wp-content/uploads/2014/01/FS-MEP_factsheet_130124.pdf

[‡] http://kiss.caltech.edu/workshops/smallsat2012b/presentations/mueller.pdf.

There are several interesting features and complexities in design of missions with significant orbit changes in Earth orbit or interplanetary orbit transfers for small satellite using SEP systems. The thrust level at a given time is a trade-off between the specific impulse, duration of the maneuver, and available energy at that point in the mission. The available power is a function of the instantaneous power from solar arrays and energy that is stored in the battery. This depends on the vehicle design (e.g. sizing of the solar panels and batteries) as well as the dynamic distance and relative angle to the sun, which is a function of the time history of the trajectory design and spacecraft orientation. Designing feasible missions is particularly challenging for spacecraft experiencing eclipses in Earth orbit or traveling away from the Sun, for example a spacecraft at Mars (0.52 AU) may receive just 44% of the amount we do at the Earth. This results in a challenging optimization problem for both the vehicle design and trajectory with a set of highly interdependent decision variables.

Literature Review

There is a large body of literature studying a variety of large and small spacecraft thrusters applied to Earth transfer and interplanetary trajectories. SEP has been proposed and used on a variety of large interplanetary missions, including optimized trajectories to the Mars surface for scientific exploration, Discovery-class mission applications, and asteroid belt missions [10, 11, 12, 13, 14]. Recent work has demonstrated the applicability of SEP solutions for optimal time and propellant solutions for operational responsiveness in LEO [15].

There is also a growing literature on systems-level approaches to address the applicability of small spacecraft thrusters for missions subject to U-class mission constraints. Past work has studied a variety of orbit transfers for U-class spacecraft with realistic systems-level constraints. The feasibility of using the MiXI thruster for a lunar CubeSat mission was demonstrated, where power, thermal, and bus subsystem sizing was considered [7]. The feasibility of escaping Earth orbit with the conventional constant thrust strategy that results in spiral-out orbit-raising trajectories using the CAT thruster on a 3U has also been demonstrated [16]. Refs. [16, 17] considered system-level limitations such as volume, mass, power management, and radiation exposure. Follow-on work compared conventional constant-thrusting spiral-out approaches to thrusting near perigee approaches [17] and demonstrated the optimal approach for different constraints and objectives [18, 19].

Most of the literature in this area has focused on designing or optimizing a single type of thruster for a single or handful of mission applications using a specific performance metric, which often differs across the literature. There is currently no work in the literature that presents a systems-level approach to the integrated trajectory and vehicle design and analysis for small spacecraft with SEP applied to broad families of Earth and beyond-Earth trajectory maneuvers using a common performance metric. Considering both vehicle design and trajectory decisions together is critical to find feasible solutions and maximize performance for these highly-constrained missions. This paper will overcome this problem by developing a common modeling framework to evaluate diverse thruster technologies across a broad range of relevant mission applications for diverse sizes of U-class systems. We will then use it to design mission architecture, and demonstrate resulting mass, volume, and orbit transfer trade-offs for different Earth and interplanetary small spacecraft missions using the CAT thruster.

Paper Overview

The goal of this paper is to evaluate the feasibility of using a small spacecraft form-factor for Earth-escape and interplanetary trajectories. We aim to establish what the key constraints and trade-offs are in these types of orbit transfers. A systems-level perspective that considers realistic vehicle as well as operational constraints is critical to ensure relevance of proposed solutions to realistic mission scenarios, particularly for U-class architectures that are extremely mass, volume, and power constrained. We develop a systems-level model that includes propulsion, orbit dynamics, and energy dynamics. The approach is used to study trajectories starting in LEO or Geostationary Earth Orbit (GEO) and make significant orbit changes (both in altitude and inclination). Second, we examine orbits starting in GEO that escape Earth orbit and travel to the Earth's Moon, Mercury, Venus, and Mars considering realistic power, mass, and volume constraints. Sensitivity analysis are performed to identify feasible mission architectures and towards understanding the key mission trade-offs. Visualization techniques will demonstrate the trade-offs and compare the performance of the various systems.

The results of this paper will help inform mission formulators, architects, system engineers, and researchers regarding the optimal thrusters for their application, constraints, and performance metrics. This paper is also intended to inform technologists which thruster properties have the greatest impact on performance in the context of realistic missions and spacecraft constraints. We also hope to inform future proposal calls about the potential to accomplish novel science or exploration investigations with small spacecraft that can achieve high ΔV Earth and interplanetary orbit transfers.

MODEL AND SPACECRAFT DESIGN

The systems-level integrated vehicle and trajectory models and simulation environment enable end-to-end design optimization of missions with SEP thrusters. The model includes analytic representations of power, structure, thermal, telecommunication, attitude control, propulsion subsystems; orbit and attitude dynamics; and environmental factors (e.g. solar, gravitational, etc.). The vehicle and mission trajectory/attitude optimization models are integrated to enhance overall mission performance.

Propulsion

The CAT propulsion system model is described in detail in Refs. [6, 18]. A general approach to model the thruster acceleration, a_t, is given by:

$$a_t = -\frac{\dot{m} V_{ex}}{m}, \tag{1}$$

$$V_{ex} = g I_{sp}, \tag{2}$$

$$\dot{m} = \delta P, \tag{3}$$

where $\dot{m}$ is the propellant flow rate, V_{ex} is the exhaust velocity, m is the spacecraft mass, g is the gravitational acceleration, and I_{sp} is the specific impulse. For CAT, $\dot{m}$ scales linearly with power, where the mass flow rate is 0.1 mg/s at 10 W. The CAT technology has a wide power range, thus can be used to achieve different amounts of thrust throughout the mission, for example adjusting to the different available power as the spacecraft travels to the inner or outer planets.

Trajectory

The orbit transfer within the Earth, Sun, and planet systems are treated separately in this section. This is because the low-thrust maneuvers in the Earth system will change the orbit over many hundreds of orbital periods, while the interplanetary transfers will occur on time scales much smaller than the periods of the final orbits.

First, we consider a spiraling out orbit trajectory in Earth orbit for an approach with constant thrusting in the velocity vector. We assume that the thrust level is sufficiently low that the orbit remains circular, which we've demonstrated is reasonable through simulations. The to-

tal ΔV for an altitude change can be computed as,

$$\Delta V = \sqrt{\frac{\mu}{r_1}} - \sqrt{\frac{\mu}{r_2}}, \tag{4}$$

where r_1 is the initial radius and r_2 is the final radius from the center of the Earth and μ is the Earth's gravitational constant.

A simplified approach to computing the total ΔV required for an inclination change is computed as,

$$\Delta V = 2v \sin\left(\frac{i_2 - i_1}{2}\right) \tag{5}$$

where v is the orbital velocity at the given altitude, i_1 is the initial inclination and i_2 is the final inclination. In this case we assume the thrusts occur at the crossing points of the initial and final orbits, for example when the orbit crosses the equator.

For interplanetary transfers, we assume the spacecraft is first boosted from its starting orbit (in GEO for conservatism) to an Earth escape trajectory, and thereafter remains roughly in the ecliptic plane. Once the spacecraft has escaped the Earth's Sphere of Influence (SOI) and is not near other bodies, we model the two-body Sun spacecraft system where there are both boost and cruise phases. During the boost phase, when the spacecraft has left Earth's SOI and is firing the engine in order to increase its distance from the Sun, it is assumed that the thrust vector is aligned with the velocity in the Sun-centered frame. This boost phase must be simulated as a system of differential equations because neither the assumption that near-instantaneous transfer maneuvers nor the assumption of a nearly circular orbit is appropriate. Aligning the thrust and velocity is a good assumption because it will result in the greatest ΔV for a fixed amount of fuel. The thrust is assumed to always be aligned with the velocity vector and the equations of motion are given in Eqs. 6-9. The rate of change of the radial velocity, v_r, tangential velocity, v_θ, and rate of change of the angular location along the orbit, θ, are given by,

$$\dot{r} = 2a_t \sqrt{\frac{r^3}{\mu}} \tag{6}$$

$$\dot{v}_r = \frac{v_\theta^2}{r} - \frac{\mu}{r^2} + a_t \sin\gamma, \tag{7}$$

$$\dot{v}_\theta = a_t \cos\gamma - v_r\theta, \tag{8}$$

$$\dot{\theta} = \frac{v_\theta}{r}, \tag{9}$$

$$\gamma = \tan^{-1}\left(\frac{v_r}{v_\theta}\right). \tag{10}$$

where μ is the gravitational constant in the Sun system, γ is the flight path angle as in Eq. 10, and a_t is the thruster acceleration as in Eq. 1, $\dot{m}$ is the mass flow rate as in Eq. 3, and m is the spacecraft mass.

We also use a second boost phase to speed the spacecraft up and approach the target. During this phase, it is assumed that the thrust vector is orthogonal to the velocity in the Sun-centered frame, where Eqs. 11-12 replace Eqs. 7-8.

$$\dot{v}_r = \frac{v_\theta^2}{r} - \frac{\mu}{r^2} - a_t \cos\gamma \tag{11}$$

$$\dot{v}_\theta = a_t \sin\gamma - v_r\theta \tag{12}$$

To achieve orbit capture around a target planet or moon, once the spacecraft has entered the target's SOI, thrusting is done in the direction orthogonal to the velocity vector, where Eqs. 13-14 replace Eqs. 7-8. Initial results for attempted captures at the Earth's Moon and planets showed that after first entering the target's SOI, the spacecraft leaves the SOI prior to capture, therefore we can not ignore the impact of the central body's gravity on this portion of the trajectory.

$$\dot{v}_r = \frac{v_\theta^2}{r} - \frac{\mu}{r^2} + a_t \sin\gamma - a_c \cos\theta, \tag{13}$$

$$\dot{v}_\theta = a_t \cos\gamma - v_r\theta + a_c \sin\theta, \tag{14}$$

$$a_c = \frac{{\mu_c}^2}{d_c}. \tag{15}$$

The gravitational pull of the central body, a_c, is given in Eq. 15, where μ_c is the gravitational constant of the central body and d_c is the distance to the central body, which varies as the spacecraft moves relative to the target body. The central body is the Earth for the Moon capture cases and the Sun for the planet capture cases.

The perihilion and aphelion of the spacecraft relative to the target body, r_p and r_a, are a function of the radius from the target, r and the orbit eccentricity, e, which are computed in Eqs. 16-20, where v is the total velocity and h is the angular momentum.

$$v = \sqrt{v_r^2 + v_\theta^2}, \tag{16}$$

$$h = v_\theta r, \tag{17}$$

$$e = \sqrt{\frac{(2\mu - rv^2)rv_r^2 + (\mu - rv^2)^2}{\mu}}, \tag{18}$$

$$r_a = \frac{h^2}{\mu(1-e)}, \tag{19}$$

$$r_p = \frac{h^2}{\mu(1+e)}. \tag{20}$$

Spacecraft Design and Scaling

This paper focuses on U-class spacecraft (e.g. CubeSat form-factor). We assume a 1U is approximately 10 cm x

10 cm x 10 cm with a mass less than 2 kg, which is used as the scaling metric for spacecraft. The applicability of small SEP technologies is explored for a range of small spacecraft flight demonstration platforms (e.g. dedicated 3-12U CubeSats). A detailed set of modeling assumptions, scaling laws, and parameters are provided in Ref. [20], which we only summarize at a high level here.

The baseline spacecraft design assumed for the missions presented assumes COTS components to enable a low mass and cost design, consistent with the CubeSat design philosophy. Many of the selected components have flight heritage in LEO and will soon have flight heritage in deep space on the upcoming Lunar Flashlight, NEAScout, and BioSentinel 6U CubeSat missions [21, 22, 23]. The Blue Canyon XB1 bus is selected as it represents the state-of-the art and is being utilized for a variety of LEO and interplanetary applications [24]. The 1U XB1[§] includes most major CubeSat subsystems including a Guidance, Navigation, and Control (GNC) system, Command and Data Handling (CDH) system, and Electric Power System (EPS), including batteries. The XB1 unit and is sized for systems up to 27U, therefore is appropriate for the missions in this paper. The XB1 system is currently developed to operate in LEO, and the design is being extended for interplanetary missions.

The active attitude determination and control system (ADCS) is required to achieve and maintain the thrust vector in the desired direction (the thrusters are assumed to be body-fixed, generally along the longest axis). The XB1 has excellent pointing knowledge and control (better than what is required for the maneuvers studied in this paper), therefore it is assumed that the thrust vector is always perfectly aligned in the desired direction. The XB1 ADCS consists of a reaction wheel assembly (RWA), internal measurement unit, magnetometer, torque rods, sun sensors, star trackers, and Global Positioning System (GPS) for missions in LEO. Conventional LEO de-saturation techniques are not feasible for interplanetary spacecraft because magnetometers can not be used beyond Earth's magnetic field. For missions beyond LEO, reaction wheel saturation is dominated by solar pressure and careful control of solar panel orientation or thrusting can overcome this challenge. The BCT XB1 system nominally has a mass of about 1200 grams, without a RWA. The RWA is sized based on the momentum, which is a function of the CubeSat mass. The RWA mass and power is a cubic function of spacecraft mass based on a curve fit from BCT wheels, see Ref. [20]. We assume the standard U-class Aluminum structure is assumed to weigh 100 grams per CubeSat U (10 cm x 10 cm x 10 cm), or $M_{max} = 100$ grams/U.

For near-Earth applications, the spacecraft is assumed to fly an S-Band or UHF transceiver, which has a mass of 80 grams. Existing UHF and S-Band radios do not currently have the capability to return data at meaningful rates to Earth on small spacecraft form-factors. Therefore, for applications beyond LEO, such as those that escape Earth orbit and operate in deep space, the Iris transponder, a low mass (500 grams), volume, and power solution for interplanetary small spacecraft. The Iris transponder communicates to the Deep Space Network (DSN) on X-Band frequencies and is used for both telecommunication and tracking/navigation (replacing the GPS for LEO applications).

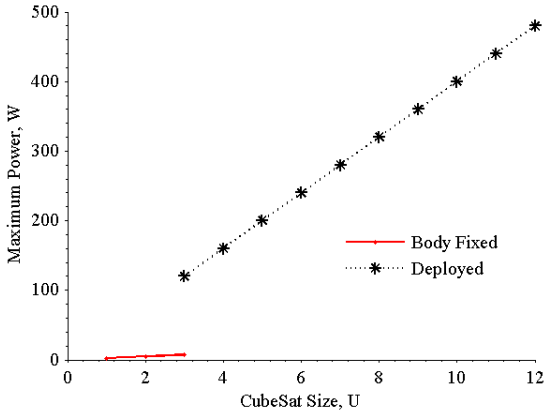

(a) Maximum Collected Power of Solar Panels

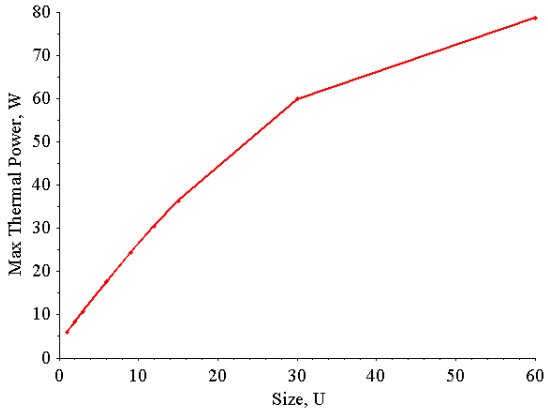

(b) Maximum Radiative Power of Radiator

Figure 1: Maximum Power scaling relationships for solar panels and radiator

[§]http://bluecanyontech.com

Ref. [20] provides a detailed description of the solar panel and radiation scaling laws for U-class spacecraft used in this paper. The solar panel maximum power values are shown in Fig. 1, where deployed panels are assumed to track the Sun [25] and the power of the body-fixed panels is scaled according to expected average Sun angles on four available sides (usually the longer ones) for representative missions. The solar panels are sized to support the bus (including RWA) and thruster simultaneously. The payload is expected to operate independently from the thruster, for example once the spacecraft reaches its destination, so the solar panels are not sized to simultaneously support the thruster and on-board instruments. The maximum heat load that can be rejected, which is a function of the maximum surface area for each U-class spacecraft size, is shown in Fig. 1b. It is assumed the system operates nearly continuously and must achieve thermal equilibrium (where the radiator is assumed to be at 40°C). Therefore, the fraction of thruster power that returns to the bus, defined as η_t, must be rejected by the radiator. Assuming constant thrusting for the mission applications, the heat that returns to the bus needs to be rejected by the radiator to maintain a thermal equilibrium. The radiator is assumed to be fixed on the largest spacecraft side, which is assumed to point towards deep space throughout all maneuvers. For spacecraft that are 3U or larger, where deployable solar panels are an option, the thermal system limits the allowable operating power of the thruster, and thus thrust level and ability to accomplish mission objectives.

A 3U spacecraft bus, not including the propulsion system, is assumed to have a volume of approximately 1.3 U based on previous work [18]. The buses scale for larger spacecraft because of larger reaction wheels, more structure, and more storage room for solar panels. Beyond-Earth missions require an additional 0.4U to accommodate the Iris transponder, which is assumed to operate at different times from the propulsion system due to thermal constraints. Overall, mass, power, and volume constraints are not modeled directly in this analysis, however conservative power and volume numbers are used and mass and volume margins are considered performance metrics.

ANALYSIS FRAMEWORK

The multi-disciplinary system-level modeling approach is demonstrated in Fig. 2, where we flow through this process for every scenario and spacecraft size we're interested in studying. This is a novel approach because the trajectory and spacecraft vehicle designs are integrated in a way that enables identifying systems-level trade-offs of multiple objectives.

First, the trajectories are defined in terms of specific impulse (I_{sp}), thrust, power ratios, mass ratios. The trajectories are defined using orbital analysis tools or defining a required ΔV to perform a certain maneuver. Second, the propulsion system is sized by determining the number of required thrusters and their power level to deliver the needed thrust that can be accommodated within the spacecraft. We assume that the spacecraft must accommodate at minimum one thruster from Table 1 due to the difficulty in scaling the technologies to even smaller systems. However, it is assumed that a fractional thruster number greater than one may be used, which represents a scaled system or different operating point. For a given spacecraft size (e.g. 6U CubeSat) we assume the initial mass is equal to the maximum allowable mass, M_{max}, and compute the required propellant mass. We assume that extended propellant tanks (as large as needed) can be accommodated and the propellant tanks are an additional 10% of the propellant mass. Third, we size the solar panels and check the feasibility of the power and thermal systems given our scaling relationships as in Fig. 1. Fourth, the spacecraft mass, M_{sc} is computed as the sum of the propulsion system mass (thruster, propellant, tank), M_{prop}, the bus mass (ADCS, EPS, radio, structure, etc.), M_{bus}, and the solar panel mass, M_{sp}, as in Eq. 21.

$$M_{sc} = M_{prop} + M_{bus} + M_{sp} \tag{21}$$

$$M_m = \frac{M_{max} - M_{sc}}{M_{max}} \cdot 100\% \tag{22}$$

$$V_m = \frac{V_{max} - V_{sc}}{V_{max}} \cdot 100\% \tag{23}$$

Fifth, the mass margin, M_m, is computed as the percentage of the remaining mass relative to the maximum allowable mass for that spacecraft size, M_{max}, as in Eq. 22. The volume margin, V_m, is computed similarly in Eq. 23, where V_{max} and V_{sc} are the maximum volume (for a given spacecraft size) and spacecraft volume, respectively.

Solutions that are found to be infeasible, in particular can not be accommodated within the spacecraft size due to mass, power, solar panel, radiator area, or volume constraints will be removed from the set of candidate solutions. Our modeling code rapidly explores this space for dozens of design points and delivers Pareto fronts showing the trade-offs between performance metrics, which are often competing. The performance metrics considered include mass and volume fractions, which provide insight into the amount of payload that can be carried, which we generally want to maximize; and the flight time, which provides insight into how quickly the maneuver can be accomplished or the destination reached,

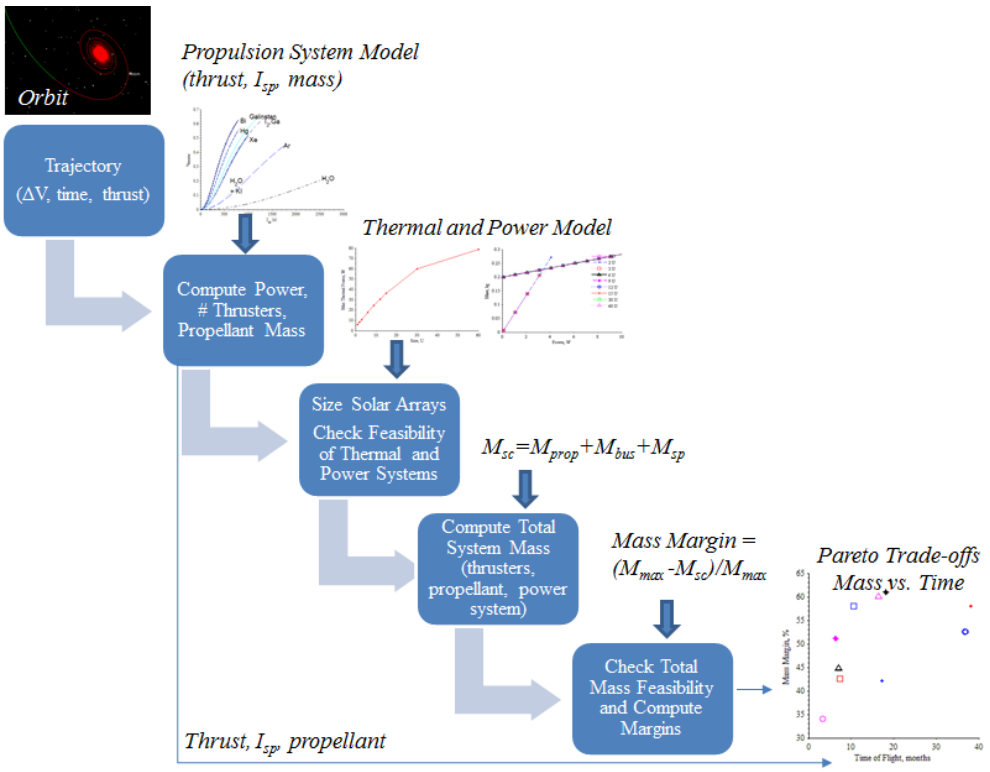

Figure 2: Modeling architecture to generate Pareto trade-offs for mission scenarios

which we generally want to minimize, particularly for small spacecraft architectures with COTS components. The duration of time the thruster is firing is often another key performance metric we want to minimize. For the LEO cases studied, the thruster is assumed to fire continuously so is equal to the orbit transfer time, while for the interplanetary cases studied, the thruster is assumed to fire continuously throughout the Earth boost, and then only during the boost phases such that the total thrust time can be extracted from the results in the following section.

THRUSTERS OVERVIEW

The SEP thrusters presented in this paper are selected based on a reasonable technology readiness level (TRL$\geq$ 5), the ability to fit and function within a 3U CubeSat (considering mass, volume, power, and thermal limitations), and the availability of information on their performance. The selected thrusters are shown in Table 1, where the values represent the system-level power, which is the power into the PPU, accounting for its inefficiencies. Note that these are only single operating points for each of the thrusters based on publicly available data and the thrusters have an operational range.

The diversity in I_{sp}, thrust and power levels are apparent in Table 1. Key thruster properties and ratios are plotted in Fig. 3. As expected, the maximum thrust to power declines with increase in I_{sp}. Most of the high thrust-to-power thrusters for a given I_{sp} (along the top descending line in Fig. 3), such as the CAT Plasma, MIT S-iEPS, and UCLA/JPL MiXI Ion thrusters are also relatively mass and volume efficient, making them attractive for small spacecraft applications [6, 26, 7]. The thrusters, PPUs, and complete systems are at various technology readiness levels, and a comparison of the system maturity is outside the scope of this paper, however another important consideration in the selection of a thruster. For example, the Busek Ion thrusters are integrated and delivered systems, while some of the other technologies are less mature at the system-level.

Throughout the rest of this paper, the CAT thruster is used in the examples due to its high performance and availability of detailed system-level technical specifications [6], however the general approach is applicable to all thrusters. The CAT thruster uses a high-density plasma source to achieve high ΔV and high thrust-to-power ratios, and fits within a small spacecraft form-factor [27, 28]. The CAT design focuses on maximizing the thrust-to-power ratio at an Isp on the lower end of electric propulsion devices. It

Table 1: Single thruster parameters for emerging small SEP technologies where the power, mass, and volume are system-level values that include the thruster, PPU, electronics, and feed system where applicable.

Thruster Name	Technology	Propellant	Power	Thrust	I_{sp}
	Units		W	mN	sec
MIT S-iEPS [26]	Electrospray	EMI-BF_4	50	2.3	2000
JPL's MEP [20]	Electrospray	Indium	8.2	0.16	3744
Busek's 0.1mN MEP [a]	Electrospray	EMI-IM	5.5	0.1	2300
Busek's 0.7mN MEP [a]	Electrospray	EMI-IM	15	0.7	800
Busek's Ion (BIT-1) [b]	Ion	Xenon	13	0.10	2150
Busek's Ion (BIT-3) [b]	Ion	Xenon	75	1.4	3500
CAT Plasma [6]	Magnetoplasma	Iodine	125	10	1010
MiXI Ion [7]	Ion	Xenon	50	1.5	3000

[a] http://busek.com/technologies__espray.htm
[b] http://busek.com/technologies__ion.htm

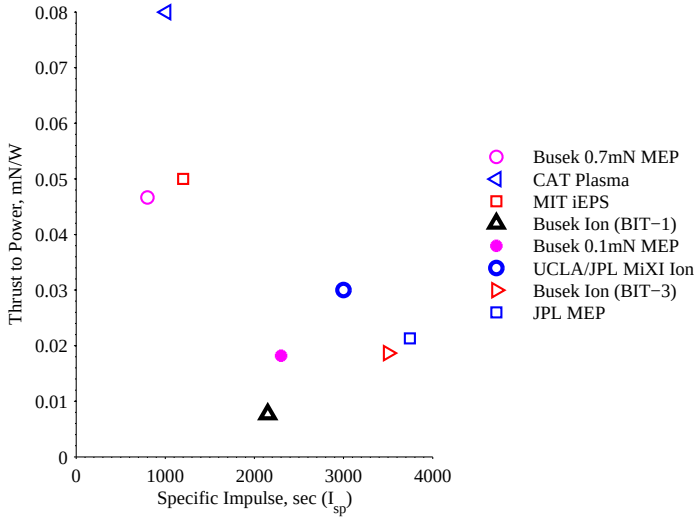

Figure 3: Thrust to power for existing and emerging small SEP thrusters

achieves a higher thrust-to-power ratio by efficiently ionizing a relatively high flow rate of propellant, about 2-3x higher flows rates than Hall effect thrusters [29]. A magnetized helicon discharge is used for this highly efficient ionization process without the need for a separate electron source such as a hollow cathode [6]. This system is designed to provide no resultant magnetic dipole. The CAT team has a dedicated NASA launch to test this thruster technology in space for the first time, and we will be collaborating with the University of Michigan and NASA Ames [30].

The CAT thruster has a system level mass and volume of 0.60 kg and 0.25 U, including the thruster, PPU, electronics, and feed system; however is still immature at the integrated systems level and the team is continuing development. We assume a single thruster is used in each spacecraft because the power levels considered are below the maximum power level of the thruster (300 W). The thruster controller is assumed to be part of the spacecraft bus and not included in these values. Although the CAT thruster can utilize a variety of propellants, we assume it uses I_2 in this paper due to its high thrust-to-power performance at reasonable I_{sp}, which has a density of about 5 g/cm^3. The CAT thruster has a highly thermal efficient and it is estimated that $\eta_t < 5\%$ (however for conservatism we use $\eta_t = 10\%$ in our modeling) of the power into the PPU becomes heat that the spacecraft bus must dissipate (using the radiators).

RESULTS

Earth Orbit Transfers

This section describes orbital transfers in Earth orbit, including both altitude and inclination changes. These

orbital transfers are of interest because small spacecraft are often launched as secondary payloads and desire different final orbits for optimal observing, to extend their lifetimes (by boosting to a higher altitude), or for operational simplicity (for example transitioning to a Sun synchronous orbit). The results from this section provide estimates for the types of payloads that can be accommodated and expected transfer times for a variety of different mission applications and spacecraft sizes.

We assume thrusting occurs with a 90% duty cycle to account for other operational constraints, including telecommunication and tracking (which may require up to 8 hrs/week or 5%), reaction wheel de-saturations, and other engineering events. We assume the time the thrusting occurs in the orbit will be selected to ensure the orbit still remains circular. This duty cycle assumption directly impacts the total time of flight (the impact of new duty cycle values can be easily computed).

Table 2: ΔV requirements for orbital transfers in Earth orbit starting from a 500 km altitude circular orbit to different final circular orbits with final altitude, A.

Parameter	Maximum LEO	GEO	Mean Moon	Earth's SOI
A (km)	2,000	35,700	384,000	919,000
ΔV (km/s)	0.6	4.4	6.5	6.9

A simple constant-thrusting maneuver is assumed, where the ΔV requirements are computed using Eqs. 4-5. The resulting transfer times and mass/volume fractions are computed using the approach represented in Fig. 2. For each case, defined by the spacecraft size and ΔV to achieve a certain orbital change, the thruster operating point (power, thrust) is selected to maximize the thrust subject to the power and thermal spacecraft constraints, which also minimizes the orbital transfer time, one of the objectives. Note that the total propellant mass (and resulting volume) is independent of the thrust level so this sizing doesn't impact the mass or volume objectives. In all of the results in this section, the Iris transponder is assumed in the vehicle design for communication and navigation due to the fact that most go beyond LEO.

The ΔV requirements for various altitude changes are summarized in Table 2. The time of flight and corresponding mass and volume margins (see Eqs. 22-23) for various altitude changes are shown in Fig. 4. Most results show significant mass and volume margins for transitions up to GEO (R =35,700 km), enabling relatively large payloads ($\geq$ 20% of maximum spacecraft mass) and/or large mass/volume system margins. In these results, the 3U spacecraft size cannot feasibly perform transfers from 500 km to altitudes exceeding 50,000 km due to mass constraints. However, there are cases where a less massive 3U spacecraft may be able to achieve this orbital maneuver with little or no payload margin.

The results for various inclination changes are in Fig. 5, where larger inclination changes are increasingly time and propellant expensive. For spacecraft at least 6U in size, it requires more time and propellant to perform a 80° inclination change than to escape Earth orbit, and therefore the mass and volume margins are lower (however first boosting to a higher altitude and performing an inclination change where the Earth gravitational pull is weaker may be advantageous). Note that performing 90° inclination changes are impossible for any of the spacecraft presented using a systems-level approach.

Transfer times and mass and volume margins improve with larger spacecraft; however there are reducing gains in these performance metrics as the spacecraft becomes more massive. The flight time improvements are because of the increase in allowable system power and therefore thrust, and the growth is minimal as both are approximately linear with increase in size. The more significant improvements in mass and volume margins with larger spacecraft are because the spacecraft bus does not increase linearly with maximum spacecraft mass/volume (only the structure and RWA mass increase). The relative increase in payload mass/volume as the spacecraft becomes larger requires multiplying the fractional values in Figs. 4c-4d by the maximum spacecraft mass/volume.

The trends in both altitude and inclination change cases are a combination of growth in maximum spacecraft mass, solar panels, radiators, spacecraft bus (e.g. RWAs grow with spacecraft size), propellant, and solar panel mass with power, which have a complex impact on mass fractions and transfer times. These results could not have been predicted without integrated system modeling.

Interplanetary Orbit Transfers

This section is an investigation of flyby and capture trajectories from GEO to Earth's Moon, Mercury, Venus, and Mars. There are emerging opportunities for small spacecraft to be launched as secondary payloads to Geostationary Transfer orbits (GTOs) and equatorial GEOs, for example through Spaceflight Services, a company that works with Launch Services Providers including SpaceX, Orbital Sciences, Virgin Galactic, Kosmotras (Dnepr), and Progress (Soyuz). There-

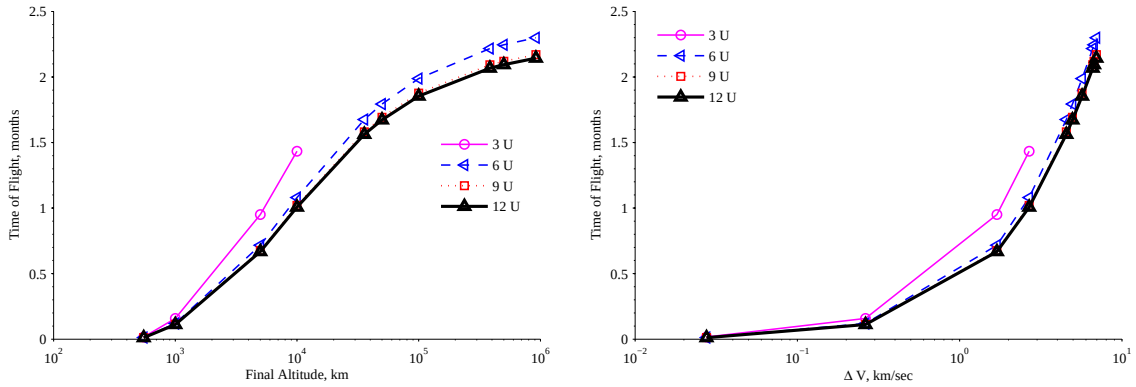

(a) Transfer Time as a function of Final Altitude

(b) Transfer Time as a function of ΔV

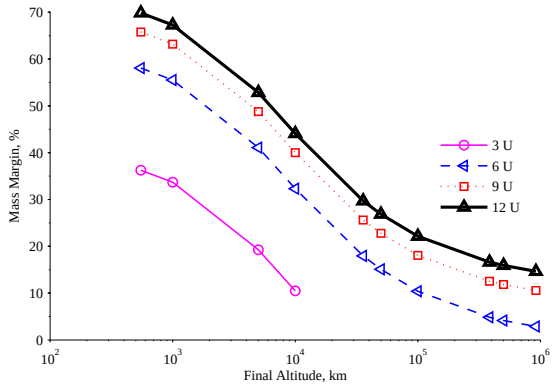

(c) Mass fraction as a function of final altitude

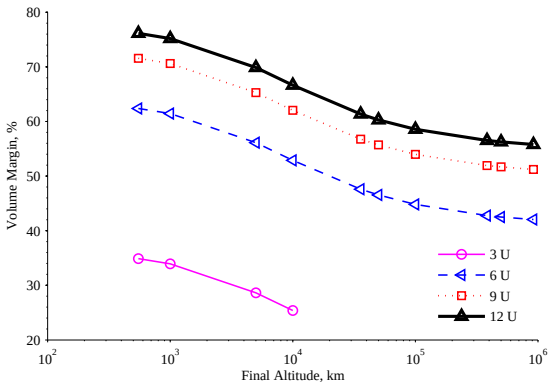

(d) Volume fraction as a function of final altitude

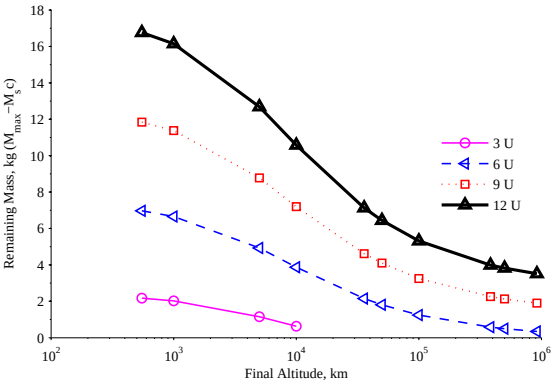

(e) Remaining mass as a function of final altitude

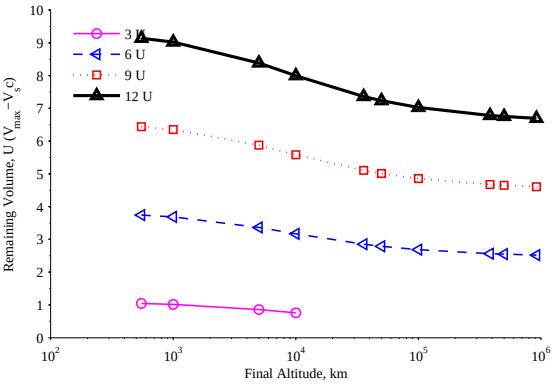

(f) Remaining volume as a function of final altitude

Figure 4: Time, mass, and volume results for altitude transfers starting from 500 km altitude circular orbit.

fore, for small spacecraft that travel to interplanetary destinations, we assume the spacecraft start in GEO, which is the more challenging case and also avoids the radiation challenges of operating in GTO with low-thrust orbit-boosting maneuvers (multiple passes through the Earth's radiation belts will result in large doses of radiation that typically cannot be survived by this class of spacecraft). Other initial and final target combinations, such as starting in LEO or Earth escape orbit ($C_3 = 0$ orbit) and targeting an interplanetary destination, can be assessed using a similar approach to the one presented in here.

The approaches described next are reasonable to achieve

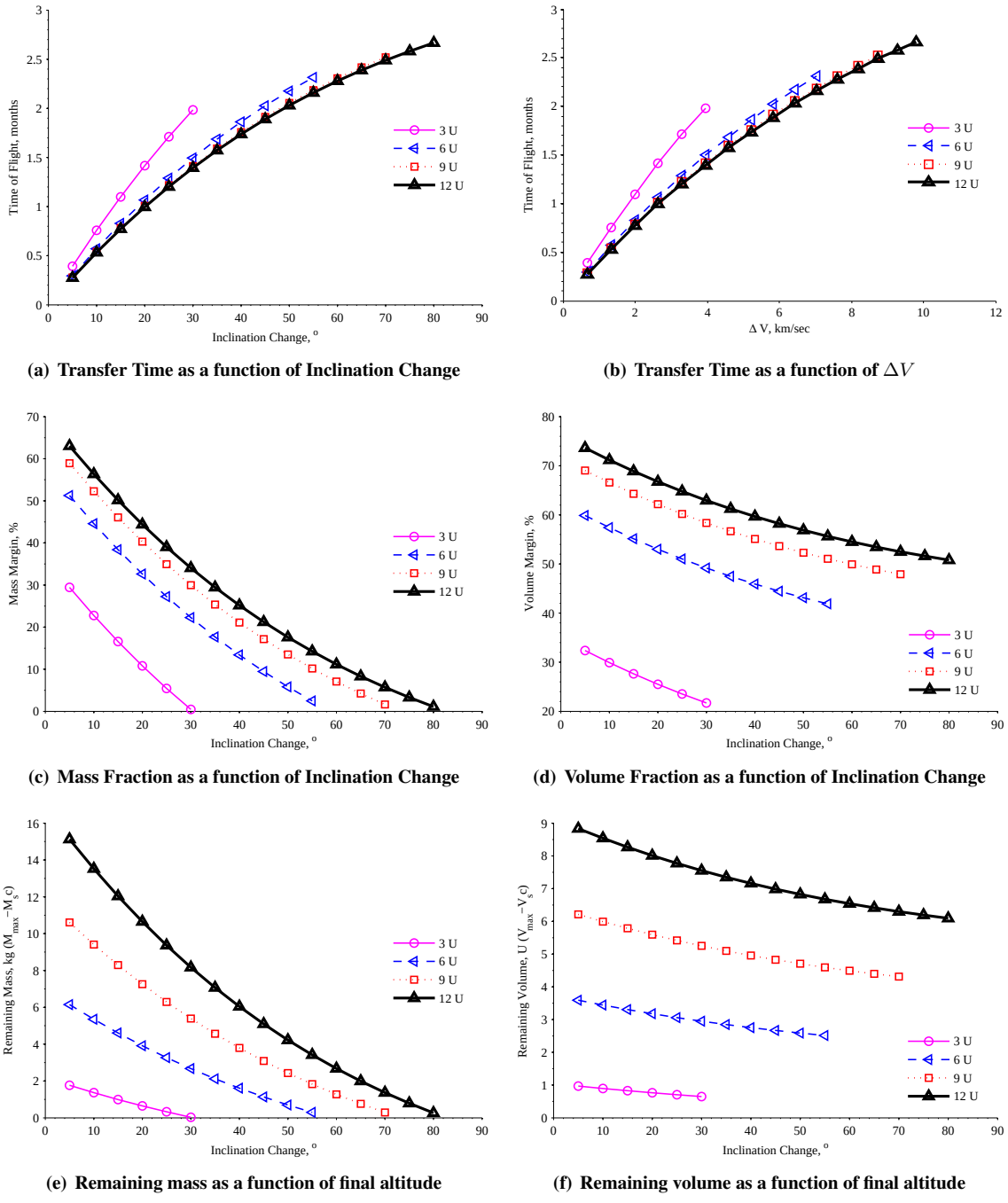

(a) Transfer Time as a function of Inclination Change

(b) Transfer Time as a function of ΔV

(c) Mass Fraction as a function of Inclination Change

(d) Volume Fraction as a function of Inclination Change

(e) Remaining mass as a function of final altitude

(f) Remaining volume as a function of final altitude

Figure 5: Time, mass, and volume results for inclination changes in a 500 km altitude circular orbit.

the flyby and capture objectives, although they are not the only feasible approaches. For orbit transfers from GEO to flybys of the Earth's Moon or a planet beyond Earth orbit, we follow these steps (shown for a Mars flyby in Fig. 6):

1. *Initialization* Start the trajectory in a circular GEO.

2. *Earth-Escape Phase* Using a two-body model where the central body is the Earth, thrust continuously in the velocity direction and altitude using Eq. 6, modeling eclipses according to the orbit altitude, as described in detail in Ref. [31]. If

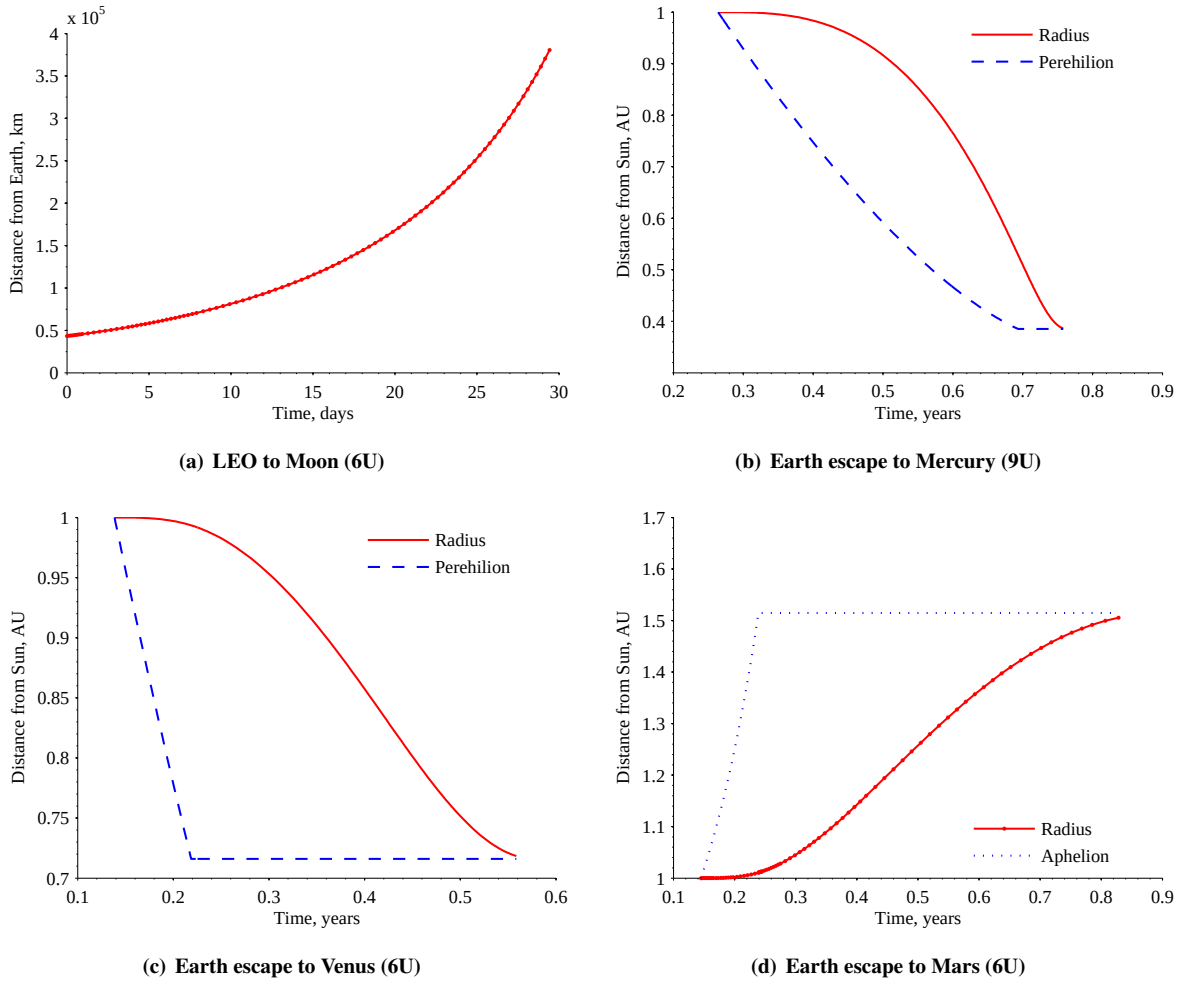

(a) LEO to Moon (6U)

(b) Earth escape to Mercury (9U)

(c) Earth escape to Venus (6U)

(d) Earth escape to Mars (6U)

Figure 7: Transfers from GEO to Earth's SOI and interplanetary bodies, assuming power generation of 70W (at 1 AU), which scales as a function of the distance to the Sun, I_2 propellant and a feasible dry spacecraft mass.

the target body is the Moon, thrust until the distance of the spacecraft relative to the Earth reaches the Moon's altitude. This will result in a flyby of the Earth's Moon and the algorithm is terminated. Alternatively, if the target body is outside the Earth's SOI, thrust until the distance of the spacecraft reaches the Earth escape altitude.

3. *Boost Phase* Using a two-body model where the central body is the Sun, thrust in the velocity direction using Eqs. 7-10, assuming there are no eclipses outside of Earth orbit. Thrust until the spacecraft's aphelion, r_a, is equal to the distance of the planet from the Sun, d.

4. *Cruise Phase* Using a two-body model where the central body is the destination planet, let the spacecraft cruise with no thrusting until the spacecraft's range from the Sun, r, is equal to the distance of the planet from the Sun, d. This will result in a flyby of the planet. Note the science observations may begin now using the available solar power.

The orbit transfer phases are shown in an example trajectory overview for a Mars flyby in Figs. 6 and the ranges over time are shown for flybys of the Moon, Mercury, Venus, and Mars in Fig. 7 and Table 3. All the systems generate 70 W (at 1 AU) and are designed to ensure a reasonable dry mass spacecraft is delivered to its destination. For the interplanetary transfers (to Mercury, Venus, and Mars), the boost phase takes a fraction of an orbit, confirming the assumptions that neither near-instantaneous transfer nor nearly circular

Table 3: Properties of trajectories that transition from GEO to *flyby* interplanetary destinations assuming I_2 propellant, no gravity assists, solar panels that generate 70W (at 1 AU), which scales as a function of the distance to the Sun, I_2 propellant and a feasible dry spacecraft mass.

Planet Destination	Moon	Mercury	Venus	Mars
Distance from Earth	384,400 km	0.39 AU	0.72 AU	0.52 AU
Available Solar Power at Target (relative to 1 AU)	44%	670 %	193 %	44%
Spacecraft Size	6U	9U	6U	9U
Travel Time: GEO to Earth's SOI	29 days	0.26 years	0.14 years	0.20 years
Travel Time: Earth's SOI to Target's SOI	n/a	0.49 years	0.42 years	0.88 years
Initial Spacecraft Mass (wet)	7.5 kg	20 kg	11 kg	16 kg
Total Propellant Mass	1.4 kg	14 kg	4.1 kg	6.9 kg

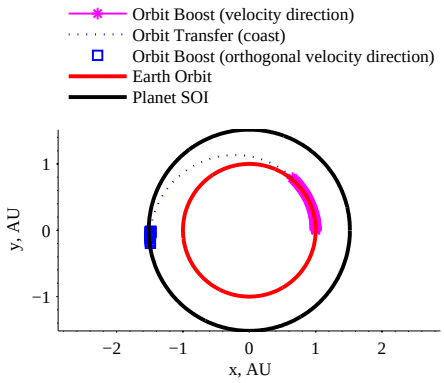

Figure 6: Trajectory from Earth escape to a Mars flyby, assuming a total initial spacecraft mass of 16 kg, the spacecraft generates a maximum power of 70 W at 1 AU, and uses I_2 propellant, as in Table 3.

orbit is appropriate to model this problem. While the engine is turned on during the boost phase, a critical metric is the spacecraft's instantaneous aphelion (r_a), which is plotted as a dotted line in Figs. 7b, 7c, and 7d. This parameter is the answer to the following question: If the spacecraft turns its engine off at that point, how great of a distance from the Sun would it attain before heading back towards Earth's orbit? As soon as the engine turns off, the spacecraft will be in an elliptic orbit about the Sun, and that orbit will have an aphelion. Once that aphelion matches the orbit of the target planet, the spacecraft has enough energy to glide on a path that will intersect the planet's orbit. When that happens, the engine turns off, and the spacecraft enters the cruise phase of the trajectory.

The available power level for continuous thrusting decreases as the orbit altitude increases from GEO to 500,000 km because the eclipse durations increase (see Ref. [18]) and the constraint that the spacecraft must be able to have a positive energy balance every orbit and not deplete on-board battery storage. When the altitude increases from 500,000 km to Earth escape (925,000 km), the eclipse durations decrease, resulting in an increase in available power (resulting in the slight increase in available power immediately before the dotted line). After the spacecraft escapes Earth orbit (dotted line), it begins the *Boost Phase* to Mars as in Fig. 6, where eclipses are no longer modeled as the spacecraft is traveling away from the Earth. After this point, the power also decreases as a function of the solar intensity decreasing as one over the distance squared (solar eclipses no longer occur during this phase).

Results for orbit trajectories from GEO to flybys of the proposed targets are summarized in Fig. 7 and Table 3. Overall flyby trajectories are feasible to all destinations studied with reasonable small spacecraft masses (still U-class form-factors) and mission times (just over a year even for the Mars transfer). Flybys of the Moon and Venus can be accomplished with a 6U, while flybys of Mercury and Mars require 9U systems. Additional studies have shown that flybys of Jupiter and Saturn require larger systems (e.g. 12U CubeSats or larger, which are not shown here) to accommodate the large required propellant volume. For each case, the spacecraft initial mass is sized to result in a reasonable dry mass and volume as in Ref. [18].

For orbit transfers from GEO to capture orbits we follow these steps (shown for a Mars capture in Fig. 8):

1. *Initialization and Earth-Escape Phases* Steps 1-2 from the flyby case. If the target is the Earth's Moon, skip to the *Capture Phase* below.

Table 4: Results for transfer from GEO to Mars capture. Results assume initial power collection of 100 W at 1 AU, an initial spacecraft mass of 15 kg, and I_2 propellant.

Phase	Description	Duration	Propellant Mass
1	Earth-Escape Boost	73 days	3.2 kg
2	Orbit Boost to Mars Orbit	34 days	3.0 kg
3	Coast to Mars Orbit	194 days	0.0 kg
4	Tangential Boost to Mars	15 days	0.6 kg
5	Mars Capture	44 days	1.8 kg
Total	GEO to Mars Capture	370 days	8.6 kg

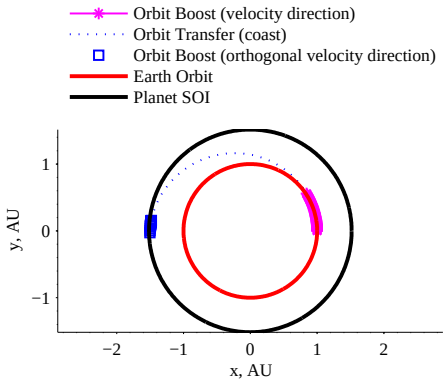

Figure 8: Trajectory from Earth escape to a Mars capture, assuming initial power collection of 100 W at 1AU, an initial spacecraft mass of 15 kg and I_2 propellant.

2. *Boost Phase* Using a two-body model where the central body is the Sun, thrust in the velocity direction and altitude using Eqs. 7-10, assuming there are no eclipses. Thrust until the spacecraft's aphelion, r_a, is equal the fraction r_f of the distance of the planet from the Sun, d, minus the destination planet's sphere of influence (SOI), d_{SOI}, i.e. $r_a = r_f(d - dSOI)$. Note this is essentially Step 3 above, but the thrusting stops prior to r_a reaching the planet's d.

3. *Cruise Phase* Using a two-body model where the central body is the Sun, let the spacecraft cruise with no thrusting until the spacecraft's range r from the destination planet is equal to a specified fraction of the distance of the planet from the Sun, d. Note this is essentially Step 4 from the flyby case, but the cruising stops prior to r reaching the distance of the planet, d.

4. *Second Boost Phase* Using a two-body model where the central body is the Sun, thrust orthogonal to the velocity direction using Eqs. 9-12. This thrusting is done until the spacecraft enters the planet's SOI, with the goal to speed up the spacecraft to approach the planet's velocity.

5. *Capture Phase* Initialize the capture by computing the total velocity relative to the target and assuming a certain entry angle, α, which is the angle between the spacecraft flight path angle and the target body's orbit. The value of α can be selected by the timing of arrival at the planet SOI, e.g. if the spacecraft arrives in front of the planet or behind it. Using a three-body model, thrust in the direction orthogonal to the velocity vector using Eqs. 9-10 and 13-15, assuming there are no eclipses. Continue thrusting until the eccentricity is below one, $e < 1$, given by Eq. 18, which represents the point where the orbit capture occurs, which results in a capture orbit about the target.

It was noted that all trajectories escaped the target's SOI after initial SOI entry before returning and achieving a capture orbit around the target. This validates that the central body's gravitational effects need to be considered (as in Eqs. 13-15), and an assumption that the spacecraft remains within the SOI of the capture target is invalid. We assume that the spacecraft does not experience solar eclipses during the capture portion about Earth's Moon.

First, we consider a low-powered 100 W transfer from GEO to Mars capture, shown in Figs. 8 and 9. We assumed an entry of $r_f = .99$ and $\alpha = 85°$, and show how the spacecraft acceleration varies as a function of power in Fig. 9d, which is a direction function of the distance from the Sun and phase. The phases of the Mars transfer from GEO to capture is summarized in Table 4, where the entire trajectory takes just over one Earth year and just less than 9 kg of propellant, which is reasonable for an initial spacecraft mass of 15 kg.

Power levels were increased to 200 W for trajectories beginning in GEO and performing orbital captures at the

Table 5: Properties of trajectories that transition from GEO to *capture* interplanetary destinations assuming I_2 propellant, solar panels that generate 150W (at 1 AU), $r_f = 1$ for the Moon and Venus and $r_f = 0.99$ for Mars (which provided the best results), $\alpha = 85°$, no gravity assists, and an appropriate dry mass to support the system.

Planet Destination	Moon	Venus	Mars
Distance from Earth	384,400 km	0.72 AU	0.52 AU
Spacecraft Size	6U	6U	9U
Travel Time: GEO to Earth's SOI	35 days	0.20 years	0.26 years
Travel Time: Earth's SOI to Target's SOI	n/a	0.52 years	0.64 years
Travel Time: Planet's SOI to Capture	2.1 days	4.8 days	21 days
Initial Spacecraft Mass (wet)	9.0 kg	15 kg	20 kg
Capture Propellant Mass	0.38 kg	1.2 kg	1.8 kg
Total Propellant Mass	2.0 kg	7.1 kg	12 kg

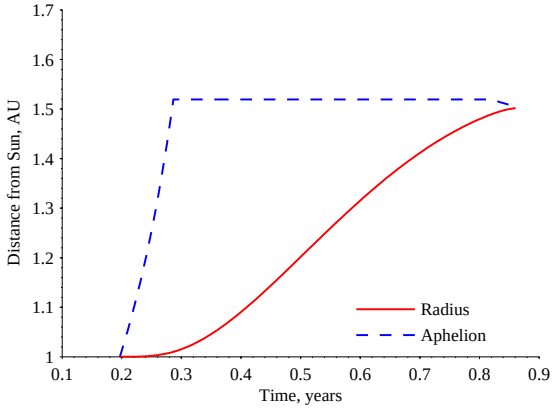

(a) Distance from Sun (GEO to pre-capture)

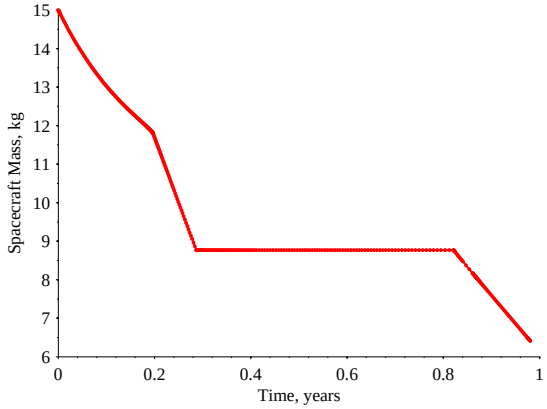

(b) Mass (GEO to Mars Capture)

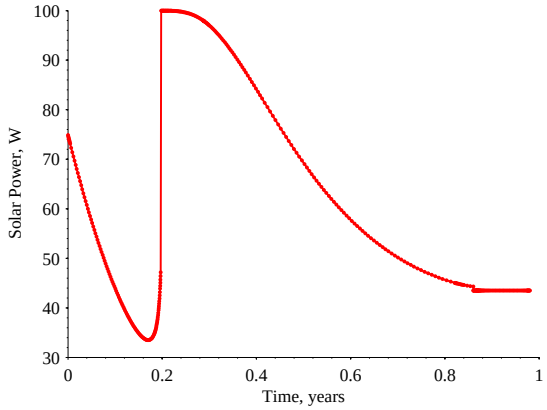

(c) Power (GEO to Mars Capture)

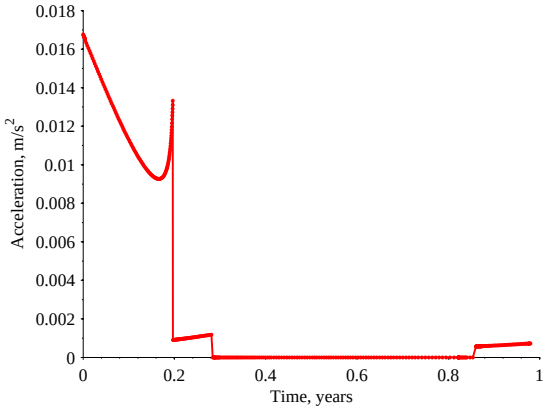

(d) Acceleration (GEO to Mars Capture)

Figure 9: Transfer time and characteristics from GEO to Mars capture, assuming initial power collection of 100 W at 1AU, an initial spacecraft mass of 15 kg, and I_2 propellant.

Earth's Moon, Mercury, Venus, and Mars, see results in Table 5. The higher power level was required because captures are particularly challenging at Mercury, Mars (as well as Jupiter and Saturn, which are not shown here). The 200 W is feasible within a 6U form-factor (or larger) using MMA's deployable HAWK solar panel technology [25], see Fig. 1a. The Mercury capture was very challenging and required a large amount of propellant, therefore is not included in these results. The trajectories and spacecraft were designed to yield reasonable final dry masses and volumes (mass is the constraint) and include the required solar panels, structure, and bus for each spacecraft design. Overall capture was feasible at all destinations; and achievable in less than one year at Venus and Mars with reasonable small spacecraft dry masses.

CONCLUSIONS

This paper addressed the challenges of performing significant interplanetary orbit trajectory changes with a small spacecraft using emerging solar electric propulsion technology. Key questions related to the feasibility of large orbital transfers in LEO and beyond LEO from a systems-level perspective have been addressed. We have identified reasonable spacecraft designs and trajectories with reasonable transfer times for representative small spacecraft form-factors to accomplish these missions.

We presented a modeling framework to enable integrated trajectory and vehicle design to enable broad solution-space exploration and evaluation of key performance trade-offs. First, a modeling framework for evaluating orbit transfers from GEO to interplanetary destinations, including propulsion, orbit, and energy dynamics was presented. Second, a simulation and optimization environment to accurately model flyby and capture trajectories to a variety of interplanetary destinations was developed. Systems-level constraints such as availability of power, energy, mass, and volume, which limit these small, highly-integrated spacecraft, have been considered. Third, these tools are used to demonstrate the feasibility for small spacecraft (focusing on 3U-9U CubeSats) to perform significant Earth orbit and interplanetary transfers using the CAT thruster technology. The approach presented is applicable to other small SEP technologies as well. The visualized results of the trade-offs between performance objectives such as mass, volume, and transfer time, provide insight for mission formulators, architects, and planners regarding the best thrusters for their application and set of constraints.

The results suggest the key limiting factor for the thrusters and scenarios studied is the thermal system, particularly when a large fraction of thruster power returns to the bus. The operating power of the propulsion system was found to be constrained by the available radiator area, which is limited for small spacecraft with small surface areas. This was particularly limiting for small 3U CubeSats, and became less constraining for 6U CubeSats and larger. This result motivates the design of optimal design of the thruster systems to return the minimal amount of heat to the bus, as well as improved thermal systems that are not constrained by the radiator surface area, for example those that use deployed radiators coupled with pumped fluid loops and/or freezable radiators.

The main results of this paper have demonstrated that it is feasible to perform significant orbital transfers in Earth orbit, including escaping Earth orbit with spacecraft larger than a 6U and performing inclination changes up to 80^{circ} with significant mass and volume margins in reasonable times (less than 3 months). We have also demonstrated that flyby and rendezvous orbital transfers from GEO to Earth's Moon, Mercury, Venus, and Mars are feasible with reasonable spacecraft masses and transfer times. Starting in GEO, flybys at Venus and Mercury are achieved in less than 0.6 and 0.8 years, respectively, with a spacecraft that collects 70 W at 1 AU. Starting in GEO, a 15 kg spacecraft generating 100 W at 1 AU achieves a capture orbit at Mars in just over one year. It is anticipated that more detailed analysis and careful planning of the trajectories, including lunar and orbital flybys, will result in improvements in transfer and capture times and spacecraft mass fractions. Overall the results presented required a strong integration between the trajectory and vehicle modeling and design, which provided important insights on what is feasible for these mission architectures.

ACKNOWLEDGMENTS

The author acknowledges Colleen Marrese-Reading, Thomas Randolf, Damon Landau, Shawn Johnson, Nitin Aurora, John Ziemer, Julie Catillo-Rogez and Andrew Gray for their contributions. Part of the research was carried out at the Jet Propulsion Laboratory, California Institute of Technology, under a contract with the National Aeronautics and Space Administration.

REFERENCES

1. Klesh, A., Baker, J., CastilloRogez, J., Halatek, L., Murphy, N., Raymond, C., Sherwood, B., Bellardo, J., Cutler, J., and Lightsey, G., "INSPIRE: Interplanetary NanoSpacecraft Pathfinder In Relevant Environment," *Proceedings of the Annual Small Satellite Conference*, Logan, Utah, August 2013.
2. Andrew D. Ketsdever, M. M. M., *Micropropulsion for Small*

Spacecraft, American Institute of Aeronautics and Astronautics, 2000.

3. Ridley, A., Forbes, J., Cutler, J., Nicholas, A., Thayer, J., Fuller-Rowell, T., Matsuo, T., Bristow, W., Conde, M., Drob, D., Paxton, L., Chappie, S., Osborn, M., Dobbs, M., Roth, J., and Armada Mission Team, "The Armada mission: Determining the dynamic and spatial response of the thermosphere/ionosphere system to energy inputs on global and regional scales," *American Geophysical Union (AGU) Fall Meeting*, Dec. 2010, pp. A7+.
4. Swenson, C., Larsen, M., Sojka, J., and Fish, C., "CubeSat Constellations for Measurements of High Latitude Energy Input," *American Geophysical Union (AGU) Fall Meeting*, Dec. 2009, pp. C1584+.
5. Mueller, J., H. R. and Ziemer, J., "Survey of propulsion technologies applicable to cubesats," *Proceedings of the 57th Joint Army-Navy-NASA-Air Force (JANNAF) Propulsion Meeting*, Colorado Springs, CO, 2010.
6. Longmier, B. and Sheehan, J. P., "Initial Experiments of a New Permanent Magnet Helicon Thruster," *International Electric Propulsion Conference*, Washington, DC, 2013.
7. Conversano, R. and Wirz, R., "CubeSat Lunar Mission Using a Miniature Ion Thruster," *47th AIAA/ASME/SAE/ASEE Joint Propulsion Conference and Exhibit*, San Diego, CA, July 2011.
8. Spangelo, S., Castillo-Rogez, J., Frick, A., Klesh, A., and Sherwood, B., "JPLs Advanced Interplanetary CubeSat Concepts for Science and Technology Demonstrations," *Interplanetary Small Satellite Conference*, Santa Clara, CA, 2015.
9. Staff, D., "Small Spacecraft Technology State of the Art," NASA/TP-2014-216648, Mission Design , Ames Research Center, Moffett Field, CA, 2014.
10. Rayman, M. D. and Williams, S. N., "Design of the First Interplanetary Solar Electric Propulsion Mission," *Journal of Spacecraft and Rockets*, Vol. 39, No. 4, 2002, pp. 589–595.
11. Williams, S. N. and Coverstone-Carroll, V., "Mars Missions Using Solar Electric Propulsion," *Journal of Spacecraft and Rockets*, Vol. 37, No. 1, 2000, pp. 71–77.
12. Oh, D. Y., "Evaluation of Solar Electric Propulsion Technologies for Discovery-Class Missions," *Journal of Spacecraft and Rockets*, Vol. 44, No. 2, 2007, pp. 399–411.
13. Schwaiger, L. E., Jr., J. M. S., Molitor, J. H., and MacPherson, D., "Solar Electric Propulsion Asteroid Belt Mission," *Journal of Spacecraft and Rockets*, Vol. 8, No. 6, 1971, pp. 612–617.
14. Snyder, J. S., Randolph, T. M., Hofer, R. R., and Goebel, D. M., "Simplified Ion Thruster Xenon Feed System For NASA Science Missions," *31st International Electric Propulsion Conference*, Ann Arbor, MI, 2009.
15. Co, T. C. and Black, J. T., "Responsiveness in Low Orbits Using Electric Propulsion," *Journal of Spacecraft and Rockets*, Vol. 51, No. 3, 2014, pp. 938–945.
16. Spangelo, S. and Longmier, B., "BravoSat: Optimizing the Delta-V Capability of a CubeSat Mission with Novel Plasma Propulsion Technology," *Interplanetary Small Satellite Conference*, Pasadena, CA, 2013.
17. Spangelo, S. and Longmier, B., "Optimizing Orbit Transfer Time using Thrust and Attitude Control for a CubeSat with Interplanetary Applications," *Interplanetary Small Satellite Conference (ISSC)*, Pasadena, CA, 2014.
18. Sara Spangelo, D. D. and Longmier, B., "Optimization of CubeSat System-Level Design and Propulsion Systems for Earth-Escape Missions," *Journal of Spacecraft and Rockets*, May 2015.
19. Kolosa, D., Spangelo, S., Lemmer, K., and Hudson, J., "Mission Analysis for a Micro RF Ion Thruster for CubeSat Orbital Maneuvers," *Joint Propulsion Conference*, Cleveland, OH, July 2014.
20. Sara Spangelo, Damon Landau, S. J. N. A. T. R., "Defining the Requirements for the Micro Electric Propulsion Systems for Small Spacecraft Missions," *Proceedings of the IEEE Aerospace Conference*, Big Sky, MT, March 2005.
21. Andreas Frick, Julie Castillo Rogez, L. J. J. D., "NEA Scout: A CubeSat Architecture for Near Earth Asteroid (NEA) Exploration," *Interplanetary Small Satellite Conference (ISSC)*, Pasadena, CA, 2014.
22. Banazadeh, P., Hayne, P., Cohe, B., and Staehle, R., "Lunar FlashLight: A CubeSat Architecture for Deep Space Exploration," 2014.
23. Sorgenfrei, M. and Lewis, B., "BioSentinel: Enabling CubeSat-Scale Biological Research Beyond Low Earth Orbit," *Interplanetary Small Satellite Conference*, Pasadena, CA, 2014.
24. (BCT), B. C. T., "XB1: High Performance 1U CubeSat Bus Specification Sheet," BCT Website, 2014.
25. VanHalle, R., "Innovative High Specific Performance (HaWK) Solar Array," *Summer CubeSat Workshop*, Logan, Utah, August 2011.
26. Francois Martel, L. P. and Lozano, P., "Miniature Ion Electrospray Thrusters and Performance Tests on CubeSats," *Proceedings of the Annual Small Satellite Conference*, Logan, Utah, August 2012.
27. Longmier, B. and Sheehan, J. P., "A New Low Power Plasma Thruster for Nanosatellites," *Joint Propulsion Conference (JPC)*, San Jose, CA, 2013.
28. Longmier, B. and Sheehan, J. P., "A Large Delta-V Plasma Thruster For Nanosatellites," *Interplanetary Small Satellite Conference*, Pasadena, CA, 2014.
29. Sheehan, J. P., Longmier, B. W., Bering, E. A., Olsen, C. S., Squire, J. P., Ballenger, M. G., Carter, M., Cassady, L. D., Daz, F. R. C., Glover, T. W., and Ilin, A. V., "Temperature Gradients Due to Adiabatic Plasma Expansion in a Magnetic Nozzle," *Plasma Sources Science and Technology*, Vol. 23, 2014.
30. Skrobot, G., "ELaNa Educational Launch of Nanosatellite: Enhance Education through Space Flight," *Proceedings of the 25th Annual Small Satellite Conference*, August 2011.
31. Sara Spangelo, D. D. and Longmier, B., "Small Spacecraft System-level Design and Optimization for Interplanetary Trajectories," *AIAA SPACE Conference*, San Diego, CA, 2014.